A Fixed Zone Perturb and Observe MPPT Technique for A Standalone Distributed PV System

Niraja Swaminathan[1], *Member, IEEE*, Lakshminarasamma N[2], *Member, IEEE* and Yue Cao[1], *Member, IEEE*

Abstract—This paper proposes a fixed zone perturb & observe (FZPO) technique to achieve an improved steady-state efficiency as well as a fast and drift-free maximum power point tracking (MPPT) for photovoltaic (PV) systems without any additional sensors. In this technique, the PV array's power-voltage curves are divided into multiple zones with unique zone boundary voltages for different irradiance conditions. This technique employs a combination of adaptive and fixed step-sizes to improve the performance, where the adaptive step-size is calculated from simple mathematical equations, resulting in a reduced computational burden. Besides, natural drift-free tracking is achieved without any additional sampling or computation, overcoming existing techniques' limitations. The FZPO technique requires a PV panel's information only at the initial design stage but not during real-time tracking, making the implementation possible using only low-cost processors. This paper presents the implementation and design of the proposed controller. The FZPO technique's performance is validated through a comprehensive set of hardware experiments on a buck-boost full-bridge converter under various irradiance conditions per the EN50530 standard. For a step-change in irradiance, the FZPO technique is experimentally verified to be 42% and 20% more efficient than the conventional and VSS techniques, respectively. During the irradiance varying conditions using the FZPO technique, the peak power loss is one-sixth compared to the conventional and VSS techniques. Practical field-related considerations such as PV panel temperature effects are further investigated through experiments.

Keywords—*Solar photovoltaics (PV), maximum power point tracking (MPPT), perturb and observe, drift-free tracking, adaptive step-size, model-based MPPT technique, steady-state oscillation, dynamic performance*

I. INTRODUCTION

SOLAR photovoltaic (PV) sources are increasing in today's electricity generation due to several advantages such as eco-friendliness, fossil fuel-free, sound-free operation, and low maintenance [1]. The PV system is constructed in either a centralized or a distributed architecture [2, 3], and the power output depends on the solar irradiance, and operating conditions [4–6]. In a centralized architecture, a single power converter is employed for the complete PV system, and therefore, maximum power is harvested using a single central maximum power point tracking (MPPT) controller. This MPPT controller must be capable of differentiating local maximum power point (LMPP), and global maximum power point (GMPP) as the power-voltage (P-V) characteristics of a solar panel array exhibit multiple maximum power points (MPPs) in the event of partial shading [2, 3, 7–11]. In contrast with the centralized architecture, the distributed architecture employs an individual DC-DC converter for each PV string, as shown in Fig. 1 and therefore, the individual MPPT controller for each PV string results in efficient tracking [2]. Besides, a simple MPPT controller suffices for a distributed architecture as the effect of partial shading is low due to individual MPP tracking of relatively small PV areas.
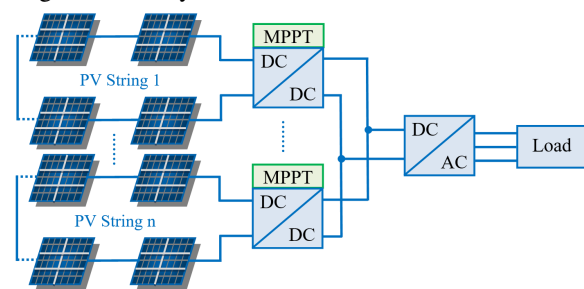
Fig. 1: An example of a distributed solar PV system

This work focuses on MPPT techniques for a standalone distributed solar PV system, demanding a low-cost and simple MPPT controller. Hill climbing MPPT techniques are well-known [4, 5, 12–18]. Among them, the conventional perturb and observe (P&O) technique is cost-effective and simple [4, 5, 13–15, 18–20]. The conventional P&O technique tracks the MPP by perturbing the control parameter based on the PV voltage and power changes. This control parameter is usually the converter's duty ratio in the direct-duty perturbation scheme or the PV voltage in the reference-voltage scheme (later Section III explains these schemes in detail). The conventional MPPT controller uses a fixed perturbation frequency and fixed step-size. Perturbation frequency defines how frequent the MPPT controller adjusts the control parameter, and a step-size is a magnitude change in the control parameter. With a large step-size, MPP tracking is fast but causes a large steady-state energy loss, while a small step-size reduces the steady-state energy loss at the cost of sluggish tracking [1, 16, 21]. Therefore, there is a compromise between the steady-state energy loss and the tracking speed under the conventional P&O technique. Incremental conductance based P&O method is presented in [20] to improve tracking speed and reduce

---
[1]Niraja Swaminathan and Yue Cao are with the School of Electrical Engineering and Computer science, Oregon State University, Corvallis, OR, USA. Niraja was previously with Indian Institute of Technology Madras, Chennai, India. E-mails: Niraja.Swaminathan@ieee.org, Yue.Cao@oregonstate.edu

[2]Lakshminarasamma N is with the Department of Electrical Engineering, Indian Institute of Technology Madras, Chennai, India. E-mail: lakshmin@ee.iitm.ac.in

energy loss compared to the conventional method. However, both techniques are prone to drift in tracking due to their operating principle.

Drift in tracking is a condition when the MPPT controller perturbs the system in the opposite direction of MPP, particularly when there is an increase in irradiance [4, 14, 17]. Although the MPPT controller eventually tracks MPP in the subsequent perturbations, the drift will be predominant when there is a continuous change in the irradiance, which is the case in the practical scenario. Besides, drift will also be prevailing with a large step-size.

To avoid the drift, the MPPT controller in [15] perturbs the system by considering the PV current changes together with the PV voltage and power changes. Some MPPT techniques in the literature eliminate the drift by using multi-sampling techniques, in which the intermediate PV voltage and current are measured to track the climatic change by subjecting the system to a small disturbance in between the usual MPPT controller perturbations [14, 22]. As a consequence, this additional disturbance increases the implementation and control complexities. Besides, the response time of the PV system limits the maximum perturbation frequency.

Adaptive step-size P&O techniques improve both steady-state efficiency and tracking speed [4, 5, 14, 19, 21–24]. One such is a variable step-size (VSS) technique [23], in which the step-size is adaptive as defined by $D_n = D_{(n-1)} \pm N * \left| \frac{P_n - P_{(n-1)}}{V_n - V_{(n-1)}} \right|$, where D is the duty of the converter, P and V are the solar panel power and voltage, and N is a scaling factor. Suffixes 'n' and '(n-1)' represent the present and previous operating points. The scaling factor "N" is determined from an experiment or a complete PV system model. Therefore, this is partially a model-based technique. In this technique, the step-size is proportional to the slope of the P-V curve, which is small and large in magnitude, on the left and right sides of the MPP point, respectively, as shown in Fig. 2(a). The VSS MPPT controller can be sluggish under a rapid decrease in irradiance due to a smaller step-size, as illustrated in Fig. 2(b). Furthermore, the VSS technique exhibits a predominant drift in tracking during an increase in irradiance, as the step-size is large when the operating point is on the right of MPP.

(a)   (b)
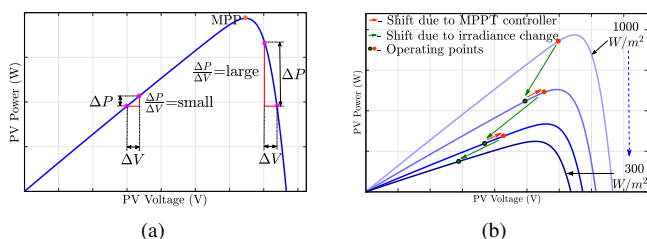
Fig. 2: P-V curves of VSS P&O technique showing (a) slope on left and right sides of the MPP, (b) the operating point moving towards left during a continuous decrease in irradiance

Ref [4] presents another adaptive P&O technique in which both the step-size and frequency of the perturbation are adaptive and are determined from the Gaussian and Arc-tangent functions involving trigonometric and exponential terms. This technique is model-based with a complicated design and requires a high-end processor. The zero-oscillation adaptive MPPT (ZA-MPPT) technique in [25] not only provides an adaptive step-size but also restricts the MPPT controller to idle when the irradiance is constant to reduce the energy loss. However, the ZA-MPPT method is not effective in practical implementation as the irradiance is not always a perfect constant. Ref [13] presents an MPPT technique using PV Power-Conductance (P-G) characteristics, where the control parameter is adjusted to match the load conductance at maximum power. However, this method does not discuss drift.

An enhanced adaptive P&O (EA-P&O) in [21] overcomes the above-mentioned limitations, such as steady-state oscillations and drift. This technique features an adaptive step-size for fast MPP tracking and reduced steady-state oscillations. Besides, the technique is capable of tracking GMPP under partial shading conditions with a reduced computational burden. However, the EA-P&O controller tracks GMPP by comparing multiple samples of perturbation, and therefore, the performance requires further validation for a fast irradiance change of 100 $W/m^2/s$, for example, as suggested by the standard EN50530 [26].

Ref [27] presents a Beta MPPT technique to track MPP based on the magnitude of a variable β instead of PV power. This technique uses a hybrid of adaptive and fixed step-sizes for fast-tracking and reduced steady-state losses. However, β and the scaling factor require manual tuning. This is overcome in [28, 29], where the parameters are auto-tuned to accommodate climatic changes. Besides, the modified Beta MPPT technique in [28] is capable of tracking the GMPP during partial shading conditions. Although Beta MPPT and its variants provide fast and efficient tracking, the β variable computation includes a logarithmic calculation.

Apart from P&O, fractional short-circuit and open-circuit techniques are other well-known MPPT techniques [14, 24, 30]. In these, drift does not exist; however, the MPPT controller interrupts the PV system periodically by opening or shorting the PV terminals for a short duration. Therefore, these are not suitable for standalone (off-grid) solar applications due to periodic service interruptions [23, 30, 31]. The use of a secondary PV cell for the PV voltage and current measurement overcomes these periodic interruptions of the primary PV system but increases the implementation cost [14].

Some model-based MPPT techniques provide overall efficient tracking. One such method tracks the MPP based on an estimation from a PV array model [32]. Unlike the P&O techniques, this one does not oscillate around the MPP, thereby improving the steady-state efficiency. Predictive control, fuzzy logic, particle swarm, and neural network [10, 11, 33–37] are some of the other model-based MPPT techniques. Model predictive control based MPPT approaches provides better steady-state and dynamic performance [34]. A polynomial fuzzy logic based technique in [36] requires a DC-DC converter model, and designing the MPPT controller is complex. One such method predicts the irradiance to track MPP, but temperature measurement is needed [37]. Ref [38] presents a model for MPP locus with temperature variations combining both the heuristic and model-based techniques. In general, most of the model-based approaches require a high-end processor to

compute sophisticated mathematical equations. Some of them are certain DC-DC converter specific, while some require temperature sensors.

As a summary of the literature review, Table I compares popular heuristic and model-based MPPT techniques based on the step-size, complexity, drift in tracking, sensor requirement, and sampling count per perturbation. Overall, the heuristic and model-based MPPT techniques presented in the literature exhibit one or more of the following limitations: (i) large energy loss at steady-state, (ii) drift in tracking, (iii) slow tracking, (iv) complicated mathematical computations, (v) multiple sampling within one MPPT tracking period, (vi) inability to track fast-changing irradiance conditions, and (vii) extra sensor/measurement. These limitations can be eliminated when the present operating point on the P-V curve is located accurately. This leads to the proposal of a zonal based MPPT technique, where the P-V curve is partitioned into multiple zones to pinpoint the operating point's location.

With the above limitations in mind, this paper proposes a fixed zone P&O technique (FZPO) for a distributed solar PV system. In this technique, P-V curves are divided into five zones, and the step-size for four zones is adaptive, while the step-size is fixed for one remaining zone. The proposed FZPO MPPT approach features: (i) improved steady-state performance, with reduced oscillations and energy loss, (ii) fast natural drift-free tracking at all operating conditions, (iii) simple mathematical equations for step-size calculation, i.e., less computational burden, (iv) no additional sampling, (v) no extra sensor, (vi) no DC-DC converter model required, and (vii) implementable even on low-end processors. Besides, the proposed FZPO technique is not converter specific and can be implemented on any DC-DC converter. This new approach requires PV panel characteristics, but only at the initialization stage.

The rest of the paper is organized as follows: Section II details the proposed FZPO theory, and Section III explains the implementation aspects and provides a design example of the FZPO controller on a DC-DC converter. In Section IV, the aforementioned features are validated by experiments in which a 200 W buck-boost full-bridge converter is chosen. The performance is compared with selected other MPPT techniques based on the start-up time, steady-state oscillations, drift occurrence, and all of these at constant, slow, and fast varying irradiances per the EN50530 standard [26]. Section V concludes this work.

II. PROPOSED FZPO TECHNIQUE

The proposed FZPO technique aims to split the P-V curves into several linear regions (zones) and employs a mix of fixed and adaptive step-sizes to improve the performance at all irradiance conditions. The FZPO technique provides a natural drift-free tracking without additional sensors or sampling, making the implementation simple.

Upcoming subsections discuss the concept, analysis, and operation of this FZPO technique.

A. Defining zones

In the FZPO technique, P-V curves are divided into multiple zones. Three is the minimum number of zones; however, at lower irradiance conditions, the tracking speed can be slow, and the linearity of the P-V curve in certain regions can be lost. Therefore, in this work, the PV curves are divided into five zones, which is the next larger zone number, as shown in Fig. 3. More than five zones increase the complexity of the algorithm. In Fig. 3, Zone 1 & Zone 5 are the non-MPP zones and are far from the MPP. Zone 3 contains the MPP, and Zone 2 & Zone 4 are the transition zones. The challenge is a mathematical definition of these zone boundaries. B_{12}, B_{23}, B_{34} and B_{45} lines represent the zone boundaries and are functions of PV voltage and current. Boundary points, where the boundary lines intercept with the irradiance curve, are represented in terms of voltages. These boundary voltages are unique to different irradiance curves to improve the proposed FZPO controller's performance since the MPP voltage is not the same at various irradiance conditions and temperatures.
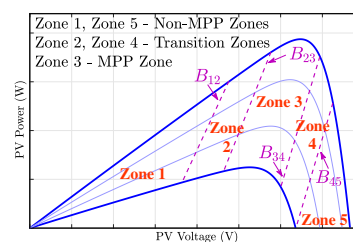
Fig. 3: P-V characteristics curve of proposed FZPO technique

The zone boundaries are defined based on the change in solar PV conductance ($\frac{\Delta P}{\Delta V^2}$) using the slope of the P-V curve versus PV voltage characteristics for the two extreme conditions, including a maximum irradiance ($1000\ W/m^2$) with a lower panel temperature ($25°C$) as well as a minimum irradiance with a higher panel temperature (per designer's choice, such as $300\ W/m^2$ and $55°C$), as shown in Fig. 4. The solar PV conductance at the two extreme conditions is obtained by plotting the P-V curve slope ($\frac{\Delta P}{\Delta V}$) versus PV voltage as shown in Fig. 5(a) and Fig. 5(b), respectively. For this, the P-V curve slope (in other words, change in power (ΔP) for a given change in voltage (ΔV)) is obtained from the solar PV model [23, 25, 39] given in (1) and (2). It is worth noting that these equations are also temperature-dependent.
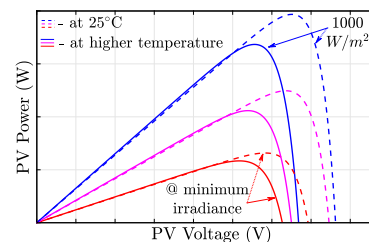
Fig. 4: P-V curves of the solar PV array at different irradiances and temperatures

TABLE I: Comparison of MPPT techniques in the literature

Techniques	Adaptive step-size	Number of sampling(s)/ perturbation	Drift-free tracking	Features
Conventional P&O	No	1	No	Simple logical comparison. Poor steady-state performance with drift in tracking.
Function-based MPPT [4]	Yes	1	Yes	Involves trigonometric and exponential computations. Requires high-end processor to compute the step-size.
Static Conductance [13]	Yes	1	No	Sophisticated mathematical equations. Involves multiple loops in the controller implementation.
Multisampling MPPT [14]	No	3	Yes	Involves multiple sampling. Does not address steady-state oscillations.
$\frac{dp}{dv}$ Method [19]	Yes	1	No	Simple logical comparison. Drift is not addressed.
Enhanced Adaptive P&O [21]	Yes	1	Yes	Simple mathematical equations. Tracks GMPP during partial shading. Tracking during fast irradiance change requires further validation.
Delta P&O, FullCurvE [22]	Yes	4	Yes	Involves multiple sampling which limits the MPPT frequency.
Variable Step-size (VSS) [23]	Yes	1	No	Simple mathematical equation. Fixed scaling factor and hence performance at certain irradiance condition is poor.
Modified Beta [28]	Yes	1	Yes	Requires logarithmic computations. Tracks GMPP during partial shading. Requires high-end processors to compute β.
MPP Estimation [32]	Yes	1	Yes	Computations with n^{th} order root. Requires high-end processor to compute the step-size.

$$I_{PV_1} = \frac{I_{ph_1} - V_{PV_1}\left[\frac{I_{sc}}{V_T} \ N_p \ e^{-\left(\frac{V_{oc\_t}}{N_s V_T}\right)} \ T_{par} + \frac{1}{R_p}\right]}{\left[1 + \frac{I_{sc}}{V_T} \ N_p \ R_s \ e^{-\left(\frac{V_{oc\_t}}{N_s V_T}\right)} \ T_{par} + \frac{R_s}{R_p}\right]} \quad (1)$$

$$\Delta P = V_{PV_1}\Delta I + I_{PV_1}\Delta V + \Delta V \Delta I \quad (2)$$

where,

$$I_{ph_1} = N_p \ \frac{G}{G_{ref}} \ (I_{sc} + [(T - T_{ref}) \cdot K_{I_{sc}}]) \quad (3)$$

$$T_{par} = \left(\frac{T}{T_{ref}}\right)^3 e^{\left(\left[\frac{1}{T_{ref}} - \frac{1}{T}\right] \frac{qE_g}{kQ_d}\right)} \quad (4)$$

$$V_{oc\_t} = (T - T_{ref}) \cdot K_{V_{oc}} + V_{oc} \quad (5)$$

where V_{PV_1}, V_{oc} and V_T are PV voltage, open-circuit voltage and thermal potential, respectively, (V); I_{PV_1}, I_{ph_1} and I_{sc} are PV current, photon current and short-circuit current, respectively, (A); N_p and N_s are numbers of parallel strings and series connected panels, respectively; R_s and R_p are series and parallel resistances of the PV array, respectively, (Ω); T_{ref} and T are reference temperature and actual temperature of the panel, respectively, (K); G_{ref} and G are reference irradiance and actual irradiance, respectively, (W/m^2); Q_d is the diode ideality factor; k is the Boltzmann's constant, (J/K); q is the coulomb constant, (C); E_g is band-energy gap, (eV); $K_{V_{oc}}$ and $K_{I_{sc}}$ are temperature coefficients of open-circuit voltage (V/°C) and short-circuit current (A/°C), respectively.

Although zones in this technique are divided based on solar array P-V curves, small variations in the parameters will not affect the performance. This is because the perturbation step size depends only on the operating PV voltage and current but not on the actual panel parameters, as presented in the

next. Therefore, accurate experimental P-V curves are not mandatory; instead, the proposed FZPO controller can be designed using the theoretical P-V curves obtained using the PV array datasheet parameters.

Using a linear curve fitting of the P-V curve slope versus PV voltage characteristics, four points are obtained on each curve at which the change in conductance occurs, as illustrated in Fig. 5(a) (at maximum irradiance) and Fig. 5(b) (at minimum irradiance). The pink dashed lines shown in Fig. 5(a) and Fig. 5(b) are used for curve fitting. The intersection points on the P-V curves define the boundary voltages. $V_{B12(max)}$, $V_{B23(max)}$, $V_{B34(max)}$, $V_{B45(max)}$ represent the zone boundary voltages at the maximum irradiance, and $V_{B12(min)}$, $V_{B23(min)}$, $V_{B34(min)}$, $V_{B45(min)}$ represent the zone boundary voltages at the minimum irradiance. After defining the boundary voltages, boundaries B_{12}, B_{23}, B_{34} and B_{45}, which are straight lines, are formed by joining the minimum and maximum boundary voltages, as shown in Fig. 5(c). As a result, the four boundary equations are defined as

$$V_{B12}(g) = V_{B23}(g) + A_1 \quad (6)$$
$$V_{B23}(g) = m_{23}I_n(g) + c_{23} \quad (7)$$
$$V_{B34}(g) = m_{34}I_n(g) + c_{34} \quad (8)$$
$$V_{B45}(g) = V_{B34}(g) + A_2 \quad (9)$$

where $I_n(g)$ is the operating PV current at irradiance 'g', (A); m_{23}, m_{34} are the slopes of boundary lines B_{23} and B_{34}, (Ω); c_{23}, c_{34} are the x-intercepts of boundary B_{23} and B_{34}, (V); A_1, A_2 are the voltage differences between the parallel boundaries B_{12} & B_{23} and B_{45} & B_{34}, (V).

Using equations (6) to (9), the FZPO controller determines boundary voltages of any operating irradiance 'g'. After determining the boundary voltages, the FZPO controller correctly identifies the operating point zone from the present PV voltage value. For example, let V_{B12} = 19.3 V, V_{B23} = 23.9 V, V_{B34} =
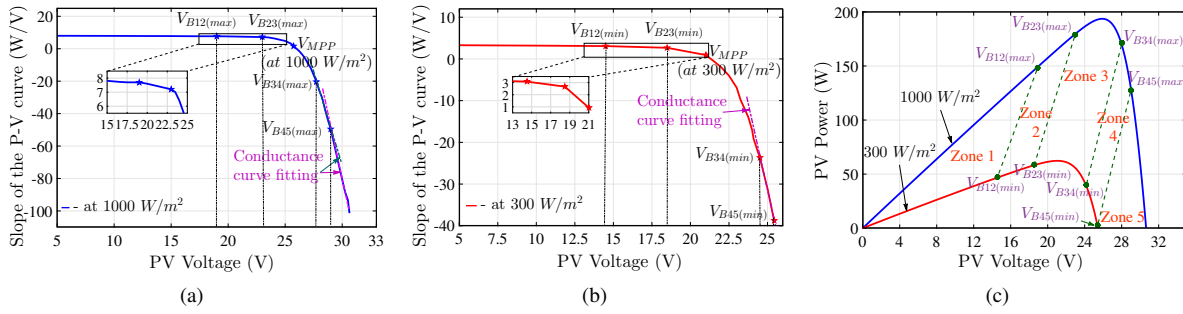
Fig. 5: (a) Slope of P-V curve vs. PV voltage for case 1 (maximum irradiance, minimum PV panel temperature), (b) Slope of P-V curve vs. PV voltage for case 2 (minimum irradiance, maximum PV panel temperature), (c) P-V curves for cases 1 and 2

25.8 V and , V_{B45} = 27 V be boundary voltages at one given condition, and let the present operating PV voltage be 24 V. In this case, the FZPO controller identifies the operating point to be in Zone 3, since the present PV voltage (24 V) is between V_{B23} and V_{B34}.

After identifying the operating zone, the FZPO controller computes the perturbation step-size for the corresponding zone, as discussed in the next subsection.

B. Mixed step-size

The FZPO technique utilizes a combination of fixed and adaptive step-sizes, depending on which zone the operating point lies in. While in Zone 3, as the operating point is in the MPP vicinity, the step-size is kept small and constant to reduce the steady-state energy loss. The working principle of the FZPO in this zone is similar to that of the conventional P&O. On the other hand, the step-size ($\Delta step$) in the remaining four zones is adaptive and computed using

$$\Delta step = m(V_n(g) - V_B(g)) + c \qquad (10)$$

where $V_B(g)$ is the boundary voltage of the adjacent zone towards the MPP at a given irradiance 'g', (V); m is the slope of the linear fitting curve, (V^{-1}); c is the y-intercept. This equation is linear as the P-V curve in these zones is almost linear.

Here the step-size $\Delta step$ is directly proportional to the difference between the present operating voltage $V_n(g)$ and the respective boundary voltage $V_B(g)$, such that the operating point moves to the next zone towards the MPP faster. Besides, the sign of $(V_n(g) - V_B(g))$ in (10) decides the direction of the perturbation, and hence no separate logic is required. It is also noted that the step size equation is independent of the PV array parameters, and therefore, the MPPT performance is not affected by the parameter variations.

C. FZPO controller operation

The flowchart in Fig. 6 presents step-by-step operations of the proposed FZPO controller. In design stages 1 and 2, the panel characteristics are fetched, zone boundaries, and step-size equations (6) to (10) are defined, as described in the above subsections. These are performed offline and are executed only once. Steps 1 to 6 are the real-time MPP tracking algorithms of the FZPO technique.
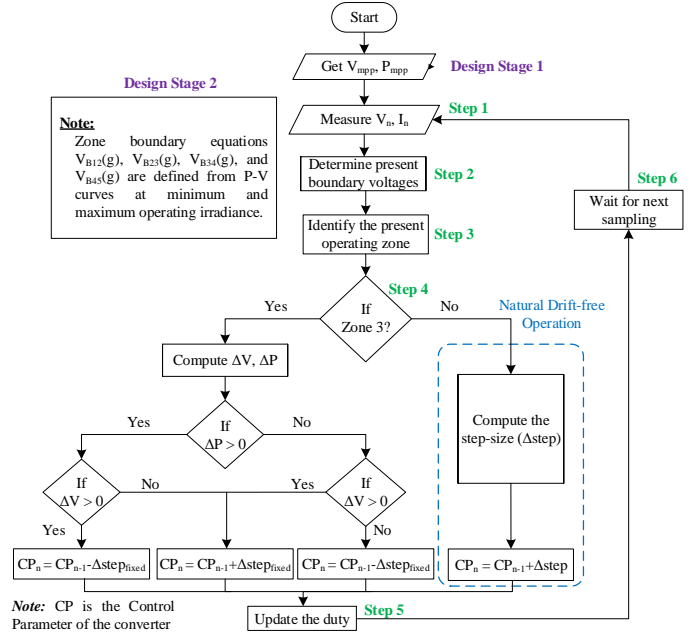
Fig. 6: Flowchart of the proposed FZPO technique

For MPP tracking, the FZPO controller measures the present operating PV voltage V_n and current I_n, as the first step. The FZPO controller then determines the zone boundary voltages for the present operating irradiance from (6) to (9), which is step 2. Once zone boundaries are determined, the FZPO controller identifies the present operating zone as step 3. Step 4 is to compute $\Delta step$. If the present operating point is already in Zone 3, $\Delta step$ is fixed. If not in Zone 3, $\Delta step$ is calculated from (10). The resultant control parameter, CP, which can be duty or phase-shift, or any other feasible parameter based on the converter, is obtained by adding (or subtracting) the $\Delta step$. As a next step, the FZPO controller updates this resultant CP in the converter and waits for the next perturbation period to measure V_n and I_n again and repeat the process.

D. Natural drift-free operation

The FZPO controller operates with natural drift-free tracking. The term natural drift-free operation in this paper is coined

as the drift is naturally eliminated due to the FZPO controller's operation, without requiring any additional algorithm.

Consider an operating point 'A' at 300 W/m^2 irradiance, as shown in Fig. 7. When the irradiance increases to 1000 W/m^2, 'A' shifts automatically to 'B,' where the load and new source curves meet (per the definition of an operating point). At this condition, the FZPO controller first identifies the 'B' zone, which is Zone 5 (per Fig. 7). Then the FZPO controller computes the step-size $\Delta step$, which is positive for this scenario as $(V_n|_{@B} - V_{B45})$ in (10) is greater than zero. The positive $\Delta step$ increments the control parameter CP, thus moving the operating point towards MPP to 'D' avoiding drift, as indicated by the green arrow in Fig. 7.
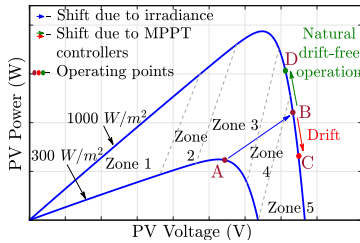
Fig. 7: Natural drift-free operation for step increase in irradiance from 300 W/m^2 to 1000 W/m^2

In some cases, the new shifted operating point can be located in Zone 3. In such conditions, though the FZPO controller behaves similarly to the conventional controller in this zone, the drift will still be negligible due to the smaller step-size. It is noted that the new operating point will be in Zone 3 mostly when there is a minimal increment in the irradiance, and hence the power loss due to the drift while in Zone 3 will be negligible.

The FZPO controller is implemented on a power converter to verify the concept and analysis presented in this section. The implementation aspects with the design example are presented in the upcoming section.

III. IMPLEMENTATION ASPECTS OF THE FZPO TECHNIQUE

To demonstrate any MPPT method, a power electronics converter is a required platform. In this work, a buck-boost full-bridge (BBFB) converter shown in Fig. 8 is chosen for implementation with the specifications mentioned in Table II. A minimum irradiance of 300 W/m^2 (which is approximately 50 W) and a maximum panel temperature of $55°C$ are considered. These numbers are just an example case for demonstration purposes. However, there is no constraint on the minimum irradiance and maximum temperature choices for FZPO. Also, the FZPO technique can be implemented on any power converter, for which the analysis presented in this work still holds.

The BBFB converter features a high gain and continuous input and output currents with high power capability [40]. In this work, BBFB is connected to a resistive load for demonstration purposes. Besides, the FZPO performance is not
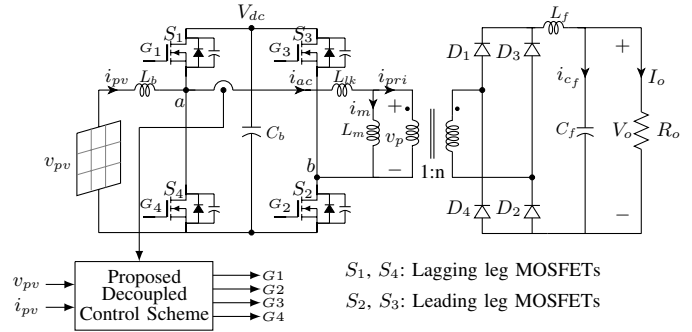
Fig. 8: Solar PV fed buck-boost full bridge converter

TABLE II: Sample parameters for the FZPO technique

Parameters	Legends	Values	Units
Solar PV MPP voltage *	V_{MPP}	25.75	V
Solar PV MPP power *	P_{MPP}	195	W
Temperature coefficient of open-circuit voltage	$K_{V_{oc}}$	-0.35	$\%/°C$
Temperature coefficient of short-circuit current	$K_{I_{sc}}$	0.05	$\%/°C$
Temperature coefficient of MPP power	$K_{P_{MPP}}$	-0.45	$\%/°C$
Load resistance	R_o	300	Ω
Irradiance range		300 - 1000	W/m^2

* At standard test conditions (STC)

affected by the load type because the MPPT controller only requires voltage and current measurements from the input side.

BBFB converter - control scheme: The BBFB converter uses a decoupled control scheme consisting of the proposed FZPO MPPT technique and a separate DC-current compensation loop [40], as shown in Fig. 9. This compensation loop mitigates the DC current in the transformer of the BBFB converter by using an asymmetrical duty control (D^*) on the leading leg MOSFETs S_2, S_3, while the duty (D) of the lagging leg MOSFETs S_1, S_4 is 50%, as shown in Fig. 9. The DC-current compensation loop's input is the transformer primary DC current ($I_{m(dc)}$), which is the difference between positive (I'_p) and negative (I''_p) transformer peak current magnitudes. The control parameter CP for the FZPO MPPT loop is the phase-shift (ϕ). Therefore, the duty reference (D^*) from the DC-current compensation loop and the phase-shift reference (ϕ) from the MPPT loop are together modulated with the ramp (carrier) signal to generate gating signals for the leading leg MOSFETs S_2 and S_3, as shown in Fig. 9.

A PI controller is sufficient for the DC-current compensation loop, since the plant transfer function is a first-order system [40], as given in

$$\frac{\hat{I}_{pri-dc}(s)}{\Delta \hat{d}(s)} = \frac{V_{PV}}{sL_m + R_{on}} \quad (11)$$

where I_{pri-dc} is the DC current in the transformer, (A); Δd is the change in duty in the leading leg MOSFETs; L_m is the magnetizing inductance, (H); R_{on} is the on-state resistance of the MOSFETs, (Ω).

The DC voltage gain (M) of the BBFB converter with this
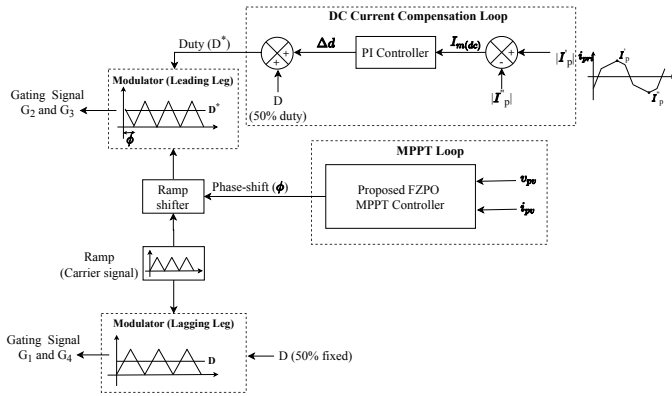
Fig. 9: Block diagram of the decoupled control scheme

control scheme is given in

$$M = \frac{2n\phi}{1 + \frac{4n^2 f_s L_{lk}}{R_o}} \quad (12)$$

where n is the transformer turns ratio; ϕ is the phase-shift of the control signal; L_{lk} is the leakage inductance of the transformer, (H); f_s is the converter switching frequency, (Hz); R_o is the load resistance, (Ω).

FZPO controller - implementation techniques: The P&O implementation is classified into reference voltage and direct-duty perturbation [5, 13, 14]. In the reference voltage perturbation scheme shown in Fig. 10(a), the MPPT controller perturbs the reference voltage (v_{ref}) based on the change in PV voltage V_{PV} and current I_{PV}. The PI controller adjusts the control parameter to match the PV voltage to the reference voltage V_{ref} [5, 13]. In this method, improved transient stability is observed, but the controller design is based on the converter model.
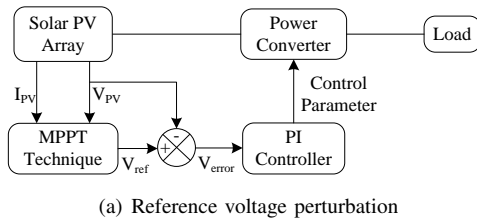
(a) Reference voltage perturbation
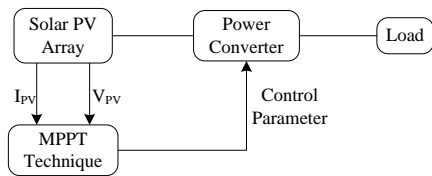
(b) Direct duty perturbation

Fig. 10: Methods of P&O implementations

In the direct-duty perturbation method shown in Fig. 10(b), the duty (or any other control parameter) of the converter is perturbed directly by the MPPT controller without requiring a PI controller [14]. Therefore, the MPPT controller design is not

converter specific. This implementation method is considered in this paper. The design of the FZPO controller parameters, based on the theory presented in the previous section, is discussed next.

FZPO controller - zone boundary equation design: Under the overall conditions from Table I, the boundary voltages at maximum and minimum irradiance conditions referring to Fig. 5(a) and Fig. 5(b) are obtained. Similarly, PV currents at these boundary voltages are obtained from Fig. 5(c) to determine the zone boundary equation constants. The design example of determining zone boundary equations (6) and (7) constants is presented below.

Design example: From Fig. 5(a) and Fig. 5(b), boundary voltages $V_{B12(max)}$, $V_{B12(min)}$, $V_{B23(max)}$ and $V_{B23(min)}$ are obtained as given in (13) and (14). Similarly, PV currents at $V_{B23(max)}$ and $V_{B23(min)}$ are obtained from Fig. 5(c) as given in (15) and (16).

$$V_{B12(max)} = 19.00\ V,\ V_{B12(min)} = 14.50\ V \quad (13)$$
$$V_{B23(max)} = 23.00\ V,\ V_{B23(min)} = 18.50\ V \quad (14)$$

$$@\ V_{B23(max)},\ I_n = 7.8\ A \quad (15)$$
$$@\ V_{B23(min)},\ I_n = 2.8\ A \quad (16)$$

Substituting above values in (7), equations (17) and (18) are obtained.

$$23 = 7.8m_{23} + c_{23} \quad (17)$$
$$18.5 = 2.8m_{23} + c_{23} \quad (18)$$

Solving (17) and (18) results in the values of constants m_{23} and c_{23} as 0.9 Ω and 15.98 V, respectively. Likewise, substituting the values of $V_{B12(max)}$ and $V_{B23(max)}$ in (6) results in constant A_1 to be $-4\ V$. Now equations (6) and (7) constants are fully determined.

Following the same procedure, constants of equations (8) and (9) are obtained. Table III presents the summary of all the zone boundary equation constants.

TABLE III: Constants of zone boundary equations

m_{23}	m_{34}	c_{23}	c_{34}	A_1	A_2
0.9 Ω	0.619 Ω	15.98 V	23.889 V	-4 V	1.25 V

For a real-time operating point, using equations (6) to (9) with the design parameters given in Table III, the proposed FZPO controller first computes all the boundary voltages based on the PV operating current and then locates the actual zone given the operating voltage. Even though the operating current may be the same across different irradiances and temperatures, the FZPO controller still identifies the operating zone accurately. To understand and validate this, consider six operating points 'A' to 'F' with the same operating current of 2.8 A at different irradiances and temperatures, as shown in Fig. 11.

For the assumed PV current of 2.8 A, the boundary voltages V_{B12} to V_{B45} are obtained from (6) to (9) as 14.5 V, 18.5 V, 25.62 V, and 26.87 V. These boundary voltages are the same
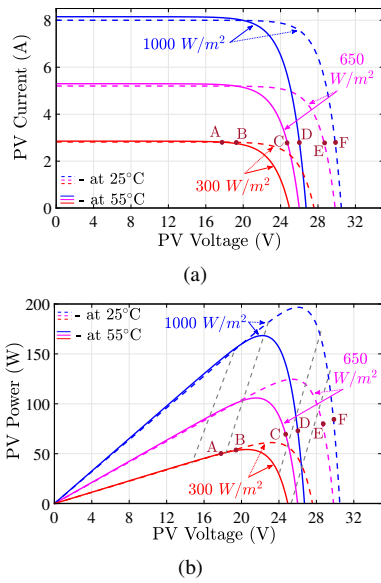
Fig. 11: (a) I-V curves at different irradiances and panel temperatures showing the operating points at the same current of 2.8 A, (b) P-V curves at different irradiances and panel temperatures showing the corresponding operating points

for all the considered operating points 'A' to 'F', as they only depend on the PV current. The FZPO controller then identifies the operating zone for each point by comparing the present operating voltage with the calculated zone boundaries. For example, the FZPO identifies the operating zone of 'A' as Zone 2 by comparing the operating voltage of 17.79 V with the corresponding calculated zone boundary voltages, i.e., between 14.5 V and 18.5 V. This is observed to be accurate from Fig. 11(b). Table IV provides the zones of 'A' to 'F' as identified by the FZPO controller (termed as "Zone - theoretical") and the actual zones identified from Fig. 11(b). It is evident that even if the PV current of all the considered points is the same, the proposed FZPO controller still identifies the zones correctly.

TABLE IV: Validation of the zone identification

Operating points	A	B	C	D	E	F
Operating PV voltage (V)	17.79	19.41	24.72	26.01	28.65	29.83
Zone - theoretical	2	3	3	4	5	5
Zone - actual	2	3	3	4	5	5

FZPO controller - step-size equation design: The adaptive step-sizes for Zones 1, 2, 4, and 5 are computed from (10). A minimum and maximum step-size for each zone defines the step-size equation constants, as discussed in the design example below.

Design example: Based on the intuitive approach, the maximum and minimum step-sizes are defined in (19) and (20).

$$Zones\ 1,\ 5 : \Delta step_{min} = 6\%,\ \Delta step_{max} = 8\% \quad (19)$$
$$Zones\ 2,\ 4 : \Delta step_{min} = 2\%,\ \Delta step_{max} = 6\% \quad (20)$$

Referring to (19), for Zone 1, when the operating point is

at 0 V, the step-size is 8%, and when it is at $V_{B12(max)}$, the step-size is 6%. It is worth noting that the step-size reduces as the operating point moves towards MPP. Substituting these conditions in (10), equations (21) and (22) are obtained.

$$-8 = m(0 - V_{B12(max)}) + c \quad (21)$$
$$-6 = m(V_{B12(max)} - V_{B12(max)}) + c \quad (22)$$

Solving (21) and (22) results in m and c values to be 0.105 and -6, respectively. Similarly, constants for the remaining zones are obtained in Table V.

TABLE V: Step-size equation constants for each zone

Constants	Zone 1	Zone 2	Zone 4	Zone 5
Slope (m) in V^{-1}	0.105	1	3.2	1
y-intercepts (c)	-6	-2	2	6
Voltage $(V_B(g))$ in V	$V_{B12}(g)$	$V_{B23}(g)$	$V_{B34}(g)$	$V_{B45}(g)$

With the above-designed parameters, the FZPO controller is ready to be implemented on the BBFB converter hardware.

IV. HARDWARE EXPERIMENTAL VALIDATION

The proposed FZPO technique is verified experimentally on a 200 W BBFB converter prototype. Experimental set-up with the specification given in Table II is shown in Fig. 12. A Chroma 62050H-600S simulator is used as the solar PV source.
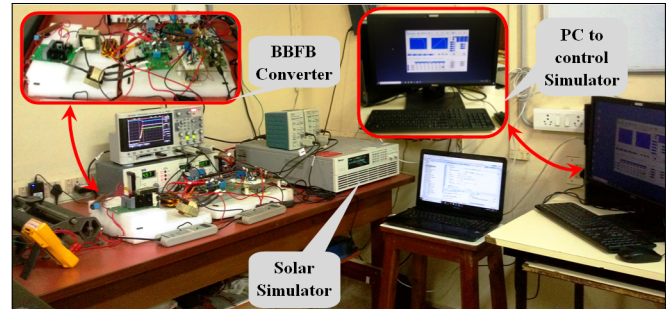
Fig. 12: Hardware experimental set-up of 200 W BBFB converter

Other MPPT techniques, such as VSS [23] and conventional P&O with similar complexity levels as that of FZPO, are also chosen for hardware implementation and side-by-side comparison. The MPPT perturbs every 1 s for all the techniques implemented in this work. The conventional P&O step-size is chosen as 4.5%. For VSS, the scaling factor N is tuned as 4 based on the design guidelines provided in [23]. For tuning N in VSS, a maximum step considered is 8%, also equivalent to that of the proposed FZPO technique.

The performance of the above-mentioned techniques is compared based on their tracking speed, steady-state oscillation, MPPT efficiency, and drifting. Additional tests are conducted at various conditions exhibiting the practical scenario, per standard EN50530 [26].

The steady-state MPPT efficiency is calculated using [26]

$$\eta_{steady-state} = \frac{P_{PV(avg)}}{P_{MPP}} \quad (23)$$

where $P_{PV(avg)}$ and P_{MPP} are the average power supplied by the PV array and the actual MPP power, respectively (W).

In general, the MPPT efficiency for any given window is computed based on the energy ratio as [26]

$$\eta_{window} = \frac{\int_{t_1}^{t_2} P_{PV}(t).dt}{\int_{t_1}^{t_2} P_{MPP}(t).dt} \tag{24}$$

where $P_{PV}(t)$ and $P_{MPP}(t)$ are the instantaneous power supplied by the PV array and the instantaneous MPP power, respectively (W); t_1 and t_2 are the lower and upper limits of the window considered (s).

Constant irradiance: The proposed FZPO technique is tested at constant irradiance of $300 \ W/m^2$, $500 \ W/m^2$ and $1000 \ W/m^2$. The results are shown in Fig. 13(a), Fig. 13(b), and Fig. 13(c), respectively. The PV voltage and current oscillations are higher at $300 \ W/m^2$ than those at $1000 \ W/m^2$ due to the constant step-size used for Zone 3. The results validate the MPP tracking at different irradiance conditions.

The FZPO technique is further tested at varying irradiance conditions as suggested in the standard EN50530, and the results are discussed further in this section.

Starting and steady-state behaviors: Two metrics, the response time to reach the steady-state at starting and the steady-state energy loss, are experimentally measured for conventional, VSS, and FZPO controllers at a constant $1000 \ W/m^2$ irradiance. The results are given in Table VI. For starting, the FZPO tracking speed is faster than the conventional and VSS techniques by 50% and 22%, respectively. For steady-state, the energy loss from the proposed FZPO is on par with the VSS approach while significantly reduced compared to the conventional method, as illustrated in the steady-state average power and MPPT efficiency values from the table.

Although the FZPO steady-state performance is not significantly better than VSS at a constant irradiance, the main advantage is observed under a dynamic irradiance change, which is discussed next.

Step increase in irradiance: The Chroma PV emulator is programmed to provide a step-change in irradiance from $300 \ W/m^2$ to $1000 \ W/m^2$ at $t = 15 \ s$ as shown in Fig. 14(a). Time taken for conventional and VSS techniques to reach steady-state is $7 \ s$ and $5 \ s$, respectively, with drift in tracking, as shown in Fig. 14(b) and Fig. 14(c), respectively. However, the proposed FZPO technique reaches the steady-state in $4 \ s$ with drift-free tracking, as shown in Fig. 14(d).

Step decrease in irradiance: For a similar experiment when a step down in irradiance from $1000 \ W/m^2$ to $300 \ W/m^2$ at $t = 15 \ s$ as shown in Fig. 15(a), the VSS performance, shown in Fig. 15(c) is observed to take $13 \ s$ to reach steady-state as its step-size is small at this transition, while the conventional technique takes only $3 \ s$ as shown in Fig. 15(b). However, the FZPO technique tracks the steady-state in only $2 \ s$, as shown in Fig. 15(d).

According to Standard EN50530 [26], the irradiance can vary at the rate of $0.5 \ W/m^2/s$ to $100 \ W/m^2/s$ in the practical scenario. A slow irradiance change (say $0.5 \ W/m^2/s$) usually does not affect MPPT's performance as the irradiance change between the tracking period is negligible. However,

a fast change in irradiance may affect MPPT's performance significantly. Therefore, to validate the performance at close-to-reality conditions, ramp sequence tests at $20 \ W/m^2/s$ and $100 \ W/m^2/s$ are presented. In some test sequences, dwell time between rise and fall of the irradiance is provided for MPPT algorithms to stabilize, as recommended in EN50530 [26].

Ramp sequence at 20 $W/m^2/s$ with 30 s dwell time: Fig. 16(a) shows the ramping irradiance with a slope of $20 \ W/m^2/s$, as recommended by EN50530 [26]. With the conventional and VSS techniques, drift is observed, particularly during the rise in irradiance, as shown in Fig. 16(b) and Fig. 16(c), respectively. Furthermore, drift is significant in VSS as the step-size is large during this test. However, the proposed FZPO operation, as shown in Fig. 16(d), does not show drift in tracking. Therefore, the experimental MPPT efficiency for the $20 \ s$ - $120 \ s$ window with the proposed FZPO technique is as high as 98.2%, while with the VSS and conventional techniques is 94.3% and 97.95%, respectively.

Ramp sequence at 100 $W/m^2/s$ with 30 s dwell time: Fig. 17(a) shows the ramping irradiance with a slope of $100 \ W/m^2/s$, as recommended by EN50530 [26]. The conventional and VSS techniques fail to track the MPP during the fast increase in irradiance and only track after the irradiance settles (after $t = 25 \ s$), as shown in Fig. 17(b) and Fig. 17(c), respectively. Meanwhile, the FZPO technique tracks the MPP even during a fast irradiance change, as shown in Fig. 17(d). The measured MPPT efficiencies of the conventional, VSS and FZPO techniques during the period of ($18 \ s$ - $62 \ s$) are 86.7%, 89.5%, and 97.85%, respectively. The power loss (p.u.) is shown in Fig. 20(a), which indicates the minimum loss with the FZPO technique. This experimental exercise unveils a good dynamic performance for the FZPO technique.

Ramp sequence varying continuously at 20 $W/m^2/s$: In the practical scenario, the irradiance tends to change continuously, particularly on partial-cloudy days. Therefore, the MPPT techniques are tested under continuously varying irradiance as recommended by EN50530 [26] with a triangular profile with a positive or negative $20 \ W/m^2/s$ slope as shown in Fig. 18(a). The conventional and VSS techniques' response shown in Fig. 18(b) and Fig. 18(c) show drift in tracking during the rise in irradiance. However, the proposed FZPO technique's performance in Fig. 18(d) reveals that the tracking is smooth even under continuously varying irradiance conditions.

Ramp sequence varying continuously at 100 $W/m^2/s$: Furthermore, the same MPPT techniques are tested under continuously varying irradiance as recommended by EN50530 [26] with a triangular profile having a positive or negative $100 \ W/m^2/s$ slope as shown in Fig. 19(a). The performance of the conventional and VSS techniques, as in Fig. 19(b) and Fig. 19(c), shows that they fail to track during continuously fast-changing irradiance. In contrast, the proposed FZPO tracks the MPP, as shown in Fig. 19(d). The power losses during ($10.5 \ s$ - $24.5 \ s$) are plotted in Fig. 20(b). It is observed that the loss is less than 10% for the FZPO technique, while it reaches as high as 70% for the conventional and VSS techniques. This particular test reveals a significant performance improvement with the FZPO technique compared to the others.

(a) $300 \ W/m^2$ (b) $500 \ W/m^2$ (c) $1000 \ W/m^2$
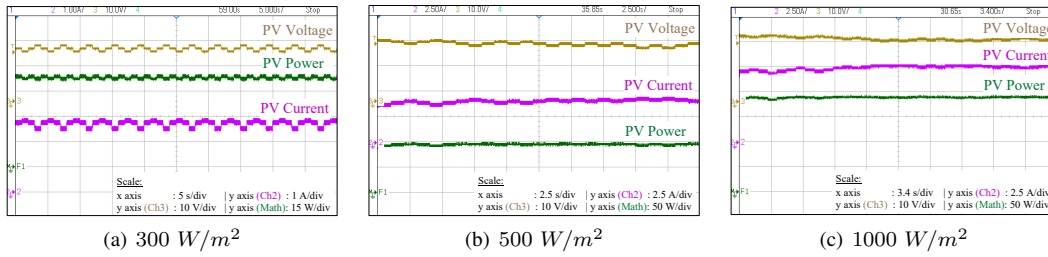
Fig. 13: Hardware experimental results of the proposed FZPO technique at constant irradiance

TABLE VI: MPPT technique performance during step-change in irradiance from $300 \ W/m^2$ to $1000 \ W/m^2$

Figure of Merits	P&O MPPT Scheme		
	Proposed	Conventional	VSS
Starting time	7 s	14 s	9 s
Average power during starting	102.62 W	89.35 W	93.69 W
MPPT efficiency during starting	52.63 %	45.82 %	48.04 %
Steady-state average power	194.76 W	192.45 W	194.69 W
MPPT efficiency during steady-state	99.88 %	98.69 %	99.85 %

(a) Test Waveform (b) Conventional P&O (c) VSS P&O (d) Proposed FZPO
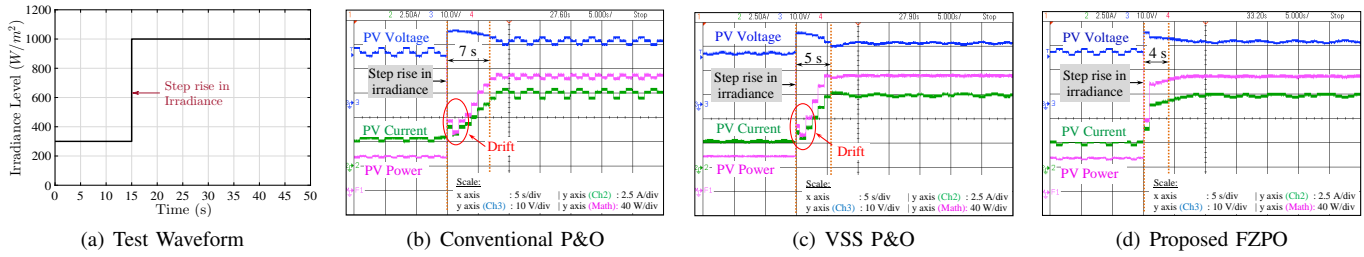
Fig. 14: Hardware experimental results: Performance with step-change in irradiance from **$300 \ W/m^2$ to $1000 \ W/m^2$** at time $t = 15 \ s$

(a) Test Waveform (b) Conventional P&O (c) VSS P&O (d) Proposed FZPO
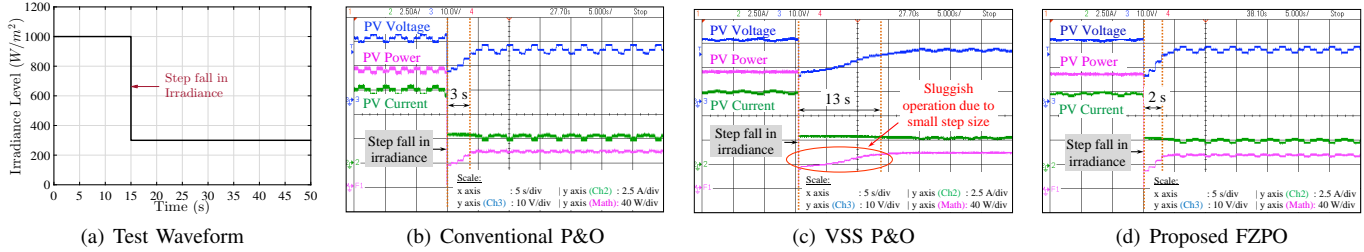
Fig. 15: Hardware experimental results: Performance with step-change in irradiance from **$1000 \ W/m^2$ to $300 \ W/m^2$** at time $t = 15 \ s$

(a) Test Waveform (b) Conventional P&O (c) VSS P&O (d) Proposed FZPO
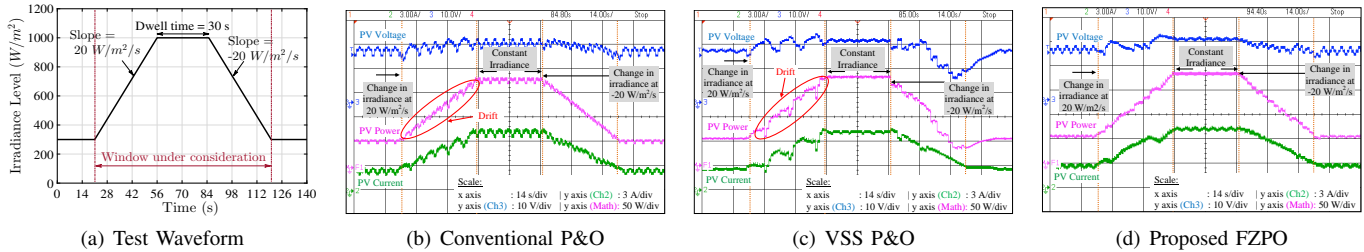
Fig. 16: Hardware experimental results: Performance with ramp test sequence (medium-high irradiance) as per EN50530 standard [26], having the slope of **$20 \ W/m^2/s$** and dwell time of $t = 30 \ s$

(a) Test Waveform   (b) Conventional P&O   (c) VSS P&O   (d) Proposed FZPO
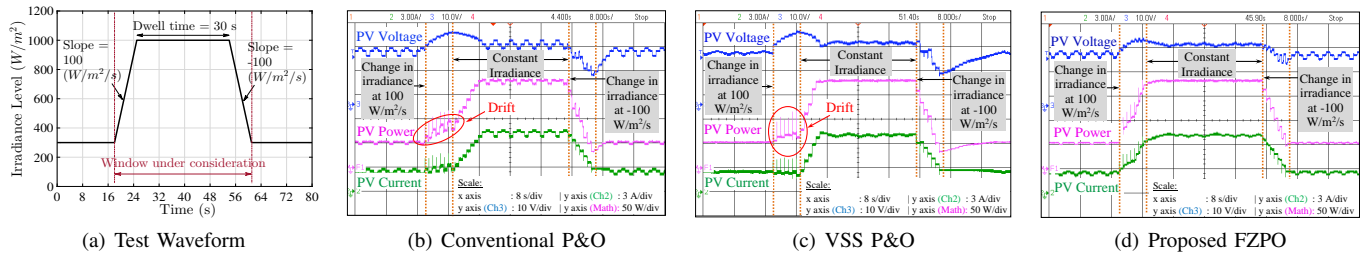
Fig. 17: Hardware experimental results: Performance with ramp test sequence (medium-high irradiance) as per EN50530 standard [26], having the slope of **100** $W/m^2/s$ and dwell time of $t = 30\ s$

(a) Test Waveform   (b) Conventional P&O   (c) VSS P&O   (d) Proposed FZPO
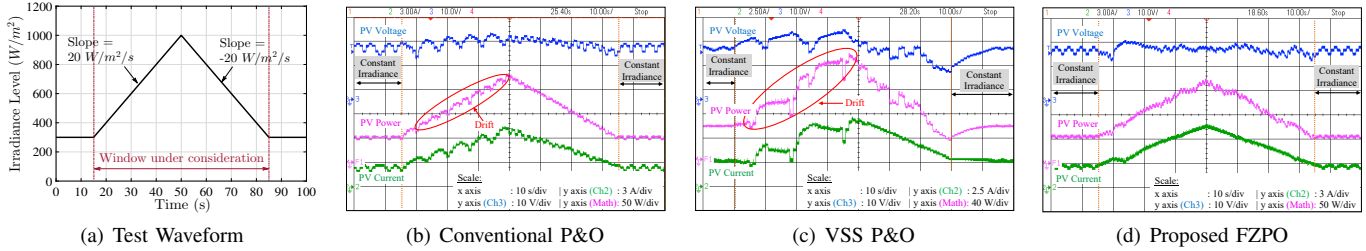
Fig. 18: Hardware experimental results: Performance with the **continuous ramp test sequence** (medium-high irradiance) per EN50530 standard [26], with a slope of $\pm$ **20** $W/m^2/s$

(a) Test Waveform   (b) Conventional P&O   (c) VSS P&O   (d) Proposed FZPO
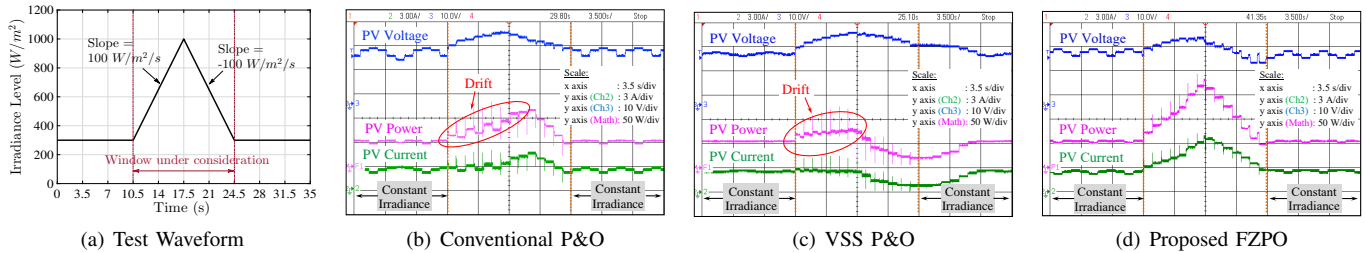
Fig. 19: Hardware experimental results: Performance with the **continuous ramp test sequence** (medium-high irradiance) as per EN50530 standard [26], with a slope of $\pm$**100** $W/m^2/s$
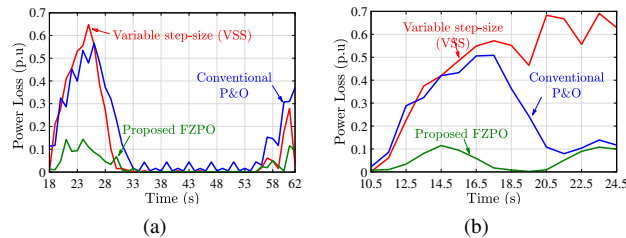
Fig. 20: Hardware experimental results: (a) Power loss during the window of (18 s - 62 s) for test waveform in Fig. 17(a), (b) Power loss during the window of (10.5 s - 24.5 s) for test waveform in Fig. 19(a)

The experimental performance of MPPT techniques at several test conditions discussed above is summarized in Table VII. It is observed that the MPPT efficiency of the FZPO technique is about 4%, 9%, and 47% higher than the VSS techniques during slow, fast, and continuously varying irradiance, respectively.

Effect of PV panel temperature variations: In a practical field-related scenario, panel temperature changes constantly, though not as fast as the irradiance does. The change in panel temperature affects the PV voltage due to a temperature coefficient of -0.35 %/°C, resulting in P-V curve shifting horizontally. Therefore, validating the proposed FZPO technique for temperature variations is necessary.

The FZPO zones are designed using (1) to (5) following the guidelines given in Section II. Fig. 21 shows the P-V curves with zones at different irradiances and panel temperatures, for the parameters given in Table II. As (1) to (5) is a function of irradiance and panel temperature, their effects are taken care of at the design stage, to ensure FZPO tracking. To verify this, the step changes between two extreme conditions, i.e., 1000 W/m^2 25°C and 300 W/m^2 55°C, are considered.

Fig. 22(a) shows the MPP tracking of the FZPO technique when subjected to a step rise in irradiance from 300 W/m^2 55°C to 1000 W/m^2 25°C. Fig. 22(b) shows the MPP tracking of the FZPO technique when subjected to a step fall in irradiance from 1000 W/m^2 25°C to 300 W/m^2 55°C. The tracking speed at these two conditions is similar to the step-change in irradiance under the uniform 25°C case. Besides, a difference of about 3.5 V in the MPP voltage at 55°C is

TABLE VII: MPPT scheme performance during dynamic irradiance conditions

Figure of Merits	P&O MPPT Scheme		
	Proposed	Conventional	VSS
Settling time with step-change in irradiance			
Step from 300 W/m^2 to 1000 W/m^2	4 s	7 s	5 s
Step from 1000 W/m^2 to 300 W/m^2	2 s	3 s	13 s
Tracking efficiency with ramp test sequence			
Slow irradiance change (20 $W/m^2/s$) with dwell time 30 s	98.2%	97.95 %	94.3%
Fast irradiance change (100 $W/m^2/s$) with dwell time 30 s	97.85%	86.7%	89.5%
Continuously varying irradiance (Triangular at 100 $W/m^2/s$)	94%	70.4 %	47.3%
Drift-free operation	Yes	No	No
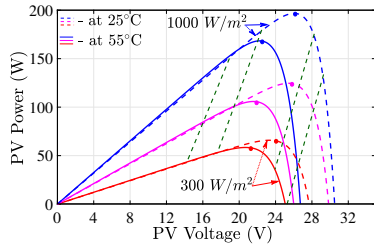
Fig. 21: P-V curves at different irradiances and temperatures indicating the MPP points and zones

observed due to the negative temperature coefficient of the PV panel material, verifying the effects of temperature change.
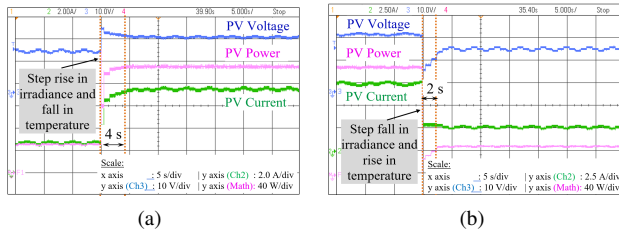
Fig. 22: Hardware experimental results of the proposed FZPO technique: (a) step-change from **1000** W/m^2 **25°C to 300** W/m^2 **55°C**, (b) step-change from **300** W/m^2 **55°C to 1000** W/m^2 **25°C**

Significant features and contributions of the FZPO technique: From the hardware experimental verification and implementation, several features, advantages, and contributions of the proposed FZPO are summarized as follows:

- The proposed zonal based technique locates the operating point irrespective of the irradiance and panel temperature variations, while most of the heuristic MPPT techniques fail to do so.
- Though the proposed FZPO technique is model-based, the design parameters are computed only once in an offline mode. At the same time, online step-size computations involve only linear equations.
- Despite being a model-based technique, the proposed FZPO does not require high-end processors due to simple computations, thereby making it cost-effective and efficient.
- The perturbation step-size in this technique is independent of the PV array and therefore, the parameter

variations in the array due to aging or other factors do not affect the performance.

- The zone boundary voltages are unique for different irradiance levels, improving the tracking speed even at a lower irradiance level.
- The mixed perturbation step-size improves both steady-state and dynamic performance.
- The perturbation step-size and the zone boundaries are defined based on linear equations, which reduce the complexity of the implementation.
- The proposed FZPO technique exhibits natural drift-free operation as the direction of perturbation is embedded in the step-size computation.
- This technique exhibits efficient tracking during slow and fast varying irradiance conditions.
- No additional sensors apart from the voltage and current sensors are required.

Limitation during partial shading: The FZPO technique is generally reliable for the distributed PV architecture, as the scope of this paper, where partial shading effect is expected low. Under a significant partial shading condition, the FZPO technique may track the GMPP with limitations. In particular, when the GMPP exhibits in Zone 3 as in Case 1 in Fig. 23, FZPO will track the point as normal. However, FZPO fails when the GMPP lies outside Zone 3, as in Case 2, when it instead tracks the LMPP in Zone 3. Besides, the FZPO algorithm may become confused when the regular GMPP and an extra LMPP both exist in Zone 3.
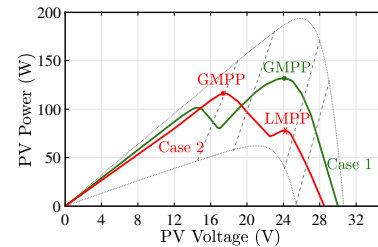
Fig. 23: Two different P-V curves during partial shading: Case 1 - FZPO successfully tracks as GMPP is located in Zone 3; Case 2 - FZPO fails to track GMPP, instead tracks LMPP that is in Zone 3

V. Conclusion

This paper proposes a fixed zone P&O (FZPO) MPPT technique to overcome the limitations, including high steady-state loss, poor dynamic performance under varying irradiance conditions, drift in tracking, multiple samplings per perturbation, need for a high-end computing processor, and need for additional temperature and irradiance sensors. In the FZPO technique, the P-V curves are divided into multiple zones, with the boundary voltages varying for different irradiance conditions. A mixed step-size with simple linear equations is employed, making the computations more efficient. Besides, the FZPO technique achieves natural drift-free tracking without an additional sampling/algorithm. The FZPO technique requires a one-time computation of the controller parameters from the PV panel information at the initial design stage. However, it does not require any complex computation during real-time tracking. The proposed FZPO converter is best suited for the standalone distributed PV systems where a low-cost, simple MPPT controller is the key requirement.

The proposed FZPO scheme is validated on a 200 W experimental prototype of a buck-boost full-bridge converter with a decoupled control scheme. The design and implementation of the MPPT controller are discussed. Several experiments present a performance comparison of the conventional, VSS, and FZPO techniques under constant/slow/fast varying irradiance conditions. Per the guidelines of Standard EN50530, the ramp change in irradiance at two different rates with and without a dwell time is tested. It is verified that even during a fast irradiance change, the proposed FZPO technique offers strong dynamic performance. The FZPO tracks the MPP with an efficiency of 42% and 20% more than the conventional and VSS techniques for a step-rise in irradiance. Similarly, the proposed FZPO technique is 24% and 47% more efficient than the conventional and VSS techniques during a continuously varying irradiance condition. Besides, under all test conditions, the FZPO provides drift-free tracking. The drift-free operating nature results in reduced power loss, particularly during the dynamic condition. The power loss plots unveil the FZPO technique having 0.1 p.u. power losses while the conventional and VSS techniques having as high as 0.6 p.u. power losses. Also, practical field-related issues such as PV panel temperature variations were investigated and experimentally validated not to affect the proposed FZPO performance.

References

[1] H. A. Sher, K. E. Addoweesh, and K. Al-Haddad, "An Efficient and Cost-Effective Hybrid MPPT Method for a Photovoltaic Flyback Microinverter," *IEEE Transactions on Sustainable Energy*, vol. 9, no. 3, pp. 1137–1144, July 2018.

[2] G. Velasco-Quesada, F. Guinjoan-Gispert, R. Pique-Lopez, M. Roman-Lumbreras, and A. Conesa-Roca, "Electrical PV Array Reconfiguration Strategy for Energy Extraction Improvement in Grid-Connected PV Systems," *IEEE Transactions on Industrial Electronics*, vol. 56, no. 11, pp. 4319–4331, Nov 2009.

[3] O. Khan and W. Xiao, "An Efficient Modeling Technique to Simulate and Control Submodule-Integrated PV System for Single-Phase Grid Connection," *IEEE Transactions on Sustainable Energy*, vol. 7, no. 1, pp. 96–107, Jan 2016.

[4] S. R. Tousi, M. H. Moradi, N. S. Basir, and M. Nemati, "A function-based maximum power point tracking method for photovoltaic systems," *IEEE Transactions on Power Electronics*, vol. 31, no. 3, pp. 2120–2128, 2016.

[5] J. Kivimaki, S. Kolesnik, M. Sitbon, T. Suntio, and A. Kuperman, "Design Guidelines for Multiloop Perturbative Maximum Power Point Tracking Algorithms," *IEEE Transactions on Power Electronics*, vol. 33, no. 2, pp. 1284–1293, Feb 2018.

[6] A. F. Murtaza, M. Chiaberge, F. Spertino, J. Ahmad, and A. Ciocia, "A Direct PWM Voltage Controller of MPPT & Sizing of DC Loads for Photovoltaic System," *IEEE Transactions on Energy Conversion*, vol. 33, no. 3, pp. 991–1001, Sept 2018.

[7] S. Selvakumar, M. Madhusmita, C. Koodalsamy, S. P. Simon, and Y. R. Sood, "High-Speed Maximum Power Point Tracking Module for PV Systems," *IEEE Transactions on Industrial Electronics*, vol. 66, no. 2, pp. 1119–1129, Feb 2019.

[8] H. Li, D. Yang, W. Su, J. Lü, and X. Yu, "An Overall Distribution Particle Swarm Optimization MPPT Algorithm for Photovoltaic System Under Partial Shading," *IEEE Transactions on Industrial Electronics*, vol. 66, no. 1, pp. 265–275, Jan 2019.

[9] J. Ahmed and Z. Salam, "An improved method to predict the position of maximum power point during partial shading for pv arrays," *IEEE Transactions on Industrial Informatics*, vol. 11, no. 6, pp. 1378–1387, 2015.

[10] I. Shams, D. S. Mekhilef, and T. Kok SOON, "Maximum power point tracking using modified butterfly optimization algorithm for partial shading, uniform shading and fast varying load conditions," *IEEE Transactions on Power Electronics*, pp. 1–1, 2020.

[11] K. Ishaque, Z. Salam, M. Amjad, and S. Mekhilef, "An improved particle swarm optimization (pso)–based mppt for pv with reduced steady-state oscillation," *IEEE Transactions on Power Electronics*, vol. 27, no. 8, pp. 3627–3638, 2012.

[12] D. Sera, R. Teodorescu, J. Hantschel, and M. Knoll, "Optimized Maximum Power Point Tracker for Fast-Changing Environmental Conditions," *IEEE Transactions on Industrial Electronics*, vol. 55, no. 7, pp. 2629–2637, July 2008.

[13] O. L. Santos, G. Garcia, L. Martinez-Salamero, R. Giral, E. Vidal-Idiarte, M. C. Merchan-Riveros, and M.-G. Yamel, "Analysis, Design and Implementation of a Static Conductance-Based MPPT Method," *IEEE Transactions on Power Electronics*, 2018.

[14] G. Escobar, S. Pettersson, C. N.-M. Ho, and R. Rico-Camacho, "Multisampling Maximum Power Point Tracker (MS-MPPT) to Compensate Irradiance and Temperature Changes," *IEEE Transactions on Sustainable Energy*, vol. 8, pp. 1096–1105, 2017.

[15] M. Killi and S. Samanta, "Modified perturb and observe MPPT algorithm for drift avoidance in photovoltaic systems," *IEEE transactions on Industrial Electronics*, vol. 62, no. 9, pp. 5549–5559, 2015.

[16] M. Lasheen, A. K. A. Rahman, M. Abdel-Salam, and S. Ookawara, "Adaptive reference voltage-based MPPT technique for PV applications," *IET Renewable Power Generation*, vol. 11, no. 5, pp. 715–722, 2017.

[17] I. G. Zurbriggen and M. Ordonez, "PV Energy Harvesting under Extremely Fast Changing Irradiance: State-plane Direct MPPT," *IEEE Transactions on Industrial Electronics*, pp. 1–1, 2018.

[18] M. Tofigh Azary, M. Sabahi, E. Babaei, and F. Abbasi Aghdam Meinagh, "Modified single-phase single-stage grid-tied flying inductor inverter with mppt and suppressed leakage current," *IEEE Transactions on Industrial Electronics*, vol. 65, no. 1, pp. 221–231, Jan 2018.

[19] H. Cai, J. Xiang, and W. Wei, "Decentralized coordination control of multiple photovoltaic sources for dc bus voltage regulating and power sharing," *IEEE Transactions on Industrial Electronics*, vol. 65, no. 7, pp. 5601–5610, 2017.

[20] Yeong-Chau Kuo, Tsorng-Juu Liang, and Jiann-Fuh Chen, "Novel maximum-power-point-tracking controller for photovoltaic energy conversion system," *IEEE Transactions on Industrial Electronics*, vol. 48, no. 3, pp. 594–601, 2001.

[21] J. Ahmed and Z. Salam, "An Enhanced Adaptive P & O MPPT for Fast and Efficient Tracking Under Varying Environmental Conditions," *IEEE Transactions on Sustainable Energy*, vol. 9, no. 3, pp. 1487–1496, July 2018.

[22] A. Pandey, N. Dasgupta, and A. K. Mukerjee, "High-Performance Algorithms for Drift Avoidance and Fast Tracking in Solar MPPT System," *IEEE Transactions on Energy Conversion*, vol. 23, no. 2, pp. 681–689, June 2008.

[23] F. Liu, S. Duan, F. Liu, B. Liu, and Y. Kang, "A Variable Step Size INC MPPT Method for PV Systems," *IEEE Transactions on Industrial Electronics*, vol. 55, no. 7, pp. 2622–2628, July 2008.

[24] S. K. Kollimalla and M. K. Mishra, "Variable Perturbation Size Adaptive P&O MPPT Algorithm for Sudden Changes in Irradiance," *IEEE Transactions on Sustainable Energy*, vol. 5, no. 3, pp. 718–728, July 2014.

[25] F. Paz and M. Ordonez, "Zero Oscillation and Irradiance Slope Tracking for Photovoltaic MPPT," *IEEE Transactions on Industrial Electronics*, vol. 61, no. 11, pp. 6138–6147, Nov 2014.

[26] EN-50530, "Overall efficiency of grid connected photovoltaic inverters," European Standard, April 2010.

[27] S. Jain and V. Agarwal, "A new algorithm for rapid tracking of approximate maximum power point in photovoltaic systems," *IEEE Power Electronics Letters*, vol. 2, no. 1, pp. 16–19, 2004.

[28] X. Li, H. Wen, Y. Hu, L. Jiang, and W. Xiao, "Modified beta algorithm for gmppt and partial shading detection in photovoltaic systems," *IEEE Transactions on Power Electronics*, vol. 33, no. 3, pp. 2172–2186, 2018.

[29] X. Li, H. Wen, L. Jiang, Y. Hu, and C. Zhao, "An improved beta method with autoscaling factor for photovoltaic system," *IEEE Transactions on Industry Applications*, vol. 52, no. 5, pp. 4281–4291, 2016.

[30] T. Hsu, H. Wu, D. Tsai, and C. Wei, "Photovoltaic Energy Harvester with Fractional Open-Circuit Voltage Based Maximum Power Point Tracking Circuit," *IEEE Transactions on Circuits and Systems II: Express Briefs*, pp. 1–1, 2018.

[31] N. Swaminathan, N. Lakshminarasamma, M. Kumaravel, and A. Jhunjhunwala, "A novel zonal based MPPT control scheme for a full bridge series resonant converter," in *2016 IEEE 43rd Photovoltaic Specialists Conference (PVSC)*, June 2016, pp. 3263–3268.

[32] M. J. Z. Zadeh and S. H. Fathi, "A New Approach for Photovoltaic Arrays Modeling and Maximum Power Point Estimation in Real Operating Conditions," *IEEE Transactions on Industrial Electronics*, vol. 64, no. 12, pp. 9334–9343, Dec 2017.

[33] Syafaruddin, E. Karatepe, and T. Hiyama, "Artificial neural network-polar coordinated fuzzy controller based maximum power point tracking control under partially shaded conditions," *IET Renewable Power Generation*, vol. 3, no. 2, pp. 239–253, June 2009.

[34] A. Lashab, D. Sera, and J. M. Guerrero, "A dual-discrete model predictive control-based mppt for pv systems," *IEEE Transactions on Power Electronics*, pp. 1–1, 2019.

[35] P. E. Kakosimos, A. G. Kladas, and S. N. Manias, "Fast photovoltaic-system voltage- or current-oriented mppt employing a predictive digital current-controlled converter," *IEEE Transactions on Industrial Electronics*, vol. 60, no. 12, pp. 5673–5685, Dec 2013.

[36] M. Rakhshan, N. Vafamand, M. Khooban, and F. Blaabjerg, "Maximum power point tracking control of photovoltaic systems: A polynomial fuzzy model-based approach," *IEEE Journal of Emerging and Selected Topics in Power Electronics*, vol. 6, no. 1, pp. 292–299, 2018.

[37] L. Cristaldi, M. Faifer, M. Rossi, and S. Toscani, "Mppt definition and validation: A new model-based approach," in *2012 IEEE International Instrumentation and Measurement Technology Conference Proceedings*, 2012, pp. 594–599.

[38] L. V. Hartmann, M. A. Vitorino, M. B. d. R. Correa, and A. M. N. Lima, "Combining model-based and heuristic techniques for fast tracking the maximum-power point of photovoltaic systems," *IEEE Transactions on Power Electronics*, vol. 28, no. 6, pp. 2875–2885, 2013.

[39] H. Tian, F. Mancilla-David, K. Ellis, E. Muljadi, and P. Jenkins, "Detailed performance model for photovoltaic systems," National Renewable Energy Lab.(NREL), Golden, CO (United States), Tech. Rep., 2012.

[40] N. Swaminathan and N. Lakshminarasamma, "Hybrid control scheme for mitigating the inherent DC-current in the transformer in buck-boost full-bridge converter for an all-electric motor drive system," *IET Power Electronics*, vol. 11, no. 8, pp. 1452–1462, 2018.

Niraja Swaminathan (Member, IEEE) received the B.E. degree in electrical and electronics engineering from Anna University affiliated college, Chennai, TN, India, in 2012, and the M.S. and Ph.D. degrees in electrical engineering from the Indian Institute of Technology Madras (IIT Madras), Chennai, TN, India, in 2019.

Dr. Swaminathan is currently a Post-Doctoral Scholar with the Energy Systems Group at Oregon State University (OSU), Corvallis, OR, USA. Before joining her Ph.D., she was a Project Associate with the Decentralized Solar PV system team at IIT Madras. Her current research interests include power converters for renewable energy and aviation applications, digital control for power converters, maximum power point tracking for solar PV, and energy-efficient green buildings.

Dr. Swaminathan was a recipient of a SERIIUS - MAGEEP award to pursue collaborative work with a SERIIUS partner organization in 2014 and was awarded the Thirteenth rank among 5418 candidates who graduated B.E in 2012 for her academic excellence. She has been an invited reviewer for several IEEE and IET Transactions and was a session chair for ECCE 2020 conference. She helped establish a joint IEEE PES/PELS Chapter at OSU in 2020.

Lakshminarasamma N (Member, IEEE) obtained her Ph.D. degree in Electrical Engineering from the Indian Institute of Science, Bangalore. She is currently a faculty in the Indian Institute of Technology Madras, Chennai, in the Department of Electrical Engineering since 2009. Prior to this, she has put in 4 years in academics; she has worked as a software engineer in I2 Technologies India Private Limited and as a systems specialist in GE Healthcare India Limited. Her areas of interest are power electronics, Switched-mode power conversion, and renewable energy systems. She has co-authored several journal papers in peer-reviewed journals, including the IEEE Transactions on Power Electronics and several premier conferences.

Yue Cao (Member, IEEE) received the B.S. degree (Hons.) in electrical engineering with a second major in mathematics from the University of Tennessee, Knoxville, TN, USA, in 2011, and the M.S. and Ph.D. degrees in electrical engineering from the University of Illinois at Urbana–Champaign (UIUC), Champaign, IL, USA, in 2013 and 2017, respectively.

Dr. Cao is currently an Assistant Professor with the Energy Systems Group at Oregon State University (OSU), Corvallis, OR, USA. Before joining OSU, he was a Research Scientist with the Propulsions Team at Amazon Prime Air in Seattle, WA, USA. He was a Power Electronics Engineer Intern with Special Projects Group at Apple Inc., Cupertino, CA, USA; Halliburton Company, Houston, TX, USA; Flanders Electric, Evansville, IN, USA; and Oak Ridge National Laboratory, TN, USA. He was a Sundaram Seshu Fellow in 2016 at UIUC, where he was a James M. Henderson Fellow in 2012. His research interests include power electronics, motor drives, and energy storage with applications in renewable energy integration and transportation electrification.

Dr. Cao received the Myron Zucker Award from the IEEE Industry Applications Society (IAS) in 2010. He was a recipient of Oregon State Learning Innovation Award for transformative education in 2020. He served as the Corresponding Technical Programs Chair of the 2016 IEEE Power and Energy Conference at Illinois (PECI). He is currently the Tutorials Chair of the 2021 IEEE Energy Conversion Congress Expo (ECCE) and the Special Sessions Chair of 2022 ECCE. He is a board member and Award Chair of IEEE Power Electronics Society (PELS) TC11 – Aerospace Power. In 2020, he helped establish an IEEE PELS Chapter at OSU. He is currently an Associate Editor for IEEE Transactions on Transportation Electrification.